RESEARCH ARTICLE

Macromolecular Materials and Engineering
Open Access
www.mame-journal.de

# Electrospun Fibers of Polyhydroxyalkanoate/Bacterial Cellulose Blends and Their Role in Nerve Tissue Engineering

*Emmanuel Asare,* Bahareh Azimi, Elona Vasili, David A. Gregory, Mahendra Raut, Caroline S. Taylor, Stefano Linari, Serena Danti, and Ipsita Roy**

**Multimaterial blends are crucial for developing scaffolds for tissue engineering. In this study, novel blend electrospun nanofibers are created by combining short-chain length polyhydroxyalkanoates (SCL-PHAs), medium-chain length polyhydroxyalkanoates (MCL-PHAs), and bacterial cellulose (BC) using the electrospinning technique. The resulting fibrous materials are characterized for their thermal properties, morphology, and cytocompatibility with NG108-15 neuronal cells. The fabricated blend nanofibers demonstrate good cytocompatibility, as indicated by trends in cell viability and neurite outgrowth in NG108-15 cells. Importantly, the inclusion of BC in the blend significantly improves the thermal stability of the polymer matrix, as confirmed by thermogravimetric analysis. This study introduces the concept of environmentally friendly and multifunctional materials, highlighting their potential for diverse applications in various scientific disciplines and industries, particularly in the field of nerve tissue engineering.**

## 1. Introduction

Pursuing advanced materials that are sustainable, widely biocompatible, and exhibit enhanced physical properties has been a challenge in contemporary material science.[1] In this context, individual biopolymers often exhibit unique, desirable properties; however, their inherent limitations can restrict their practical utility. In response to these challenges, innovative approaches such as blending have emerged as effective strategies for maximizing the full potential of these materials.[2,3]

Biocompatible nanofibers have gained significant attention as advanced materials in tissue engineering due to their unique properties. These materials offer porosity, high surface area, material versatility, and morphological similarities to the natural extracellular matrix, promoting cell attachment and proliferation, gaseous ($O_2$, $CO_2$) exchange, and nutrient transport.[4] Moreover, electrospun nanofibers' physical and chemical characteristics can be tailored by incorporating other materials and bioactive substances for specific biological responses.[4,5] This makes the nanofibers particularly appealing for peripheral nerve regeneration, where they are expected to serve as outer tube materials or offer guidance for regenerating nerves as internal structures[6] and for wound healing applications.[4] Electrospinning is one of the established methods for producing fibers and can result in the production of fibers with diameters ranging from the nanometer to the micrometer scale.[4,7,8] Pressurized gyrospinning is another well-known technique that can lead to the efficient production of fibers of varying diameters.[9,12]

A wide range of natural and synthetic polymers have been electrospun for various applications, including tissue engineering, wound dressing, and drug delivery.[5,10,12–14] Polyhydroxyalkanoates (PHAs) are natural biopolymers that are polyesters of hydroxyalkanoic acids.[11] They are synthesized and stored in the cytoplasm of numerous prokaryotes as granules.[2,15] PHAs are typically produced through the fermentation processes, often in nutrient-limiting conditions.[16] These biodegradable polymers are polyesters containing various monomeric units. The composition of these units in each instance is regulated by the bacterial metabolic pool and the substrate specificity of the PHA synthase enzyme.[17] PHAs are categorized based on the number of carbon atoms in the monomeric unit, with short-chain length (SCL) PHAs having three to five carbon atoms and

E. Asare, D. A. Gregory, M. Raut, C. S. Taylor, I. Roy
School of Chemical
Materials and Biological Engineering
Faculty of Engineering
University of Sheffield
Sheffield S102TN, UK
E-mail: easare1@sheffield.ac.uk, emmansare1@gmail.com; i.roy@sheffield.ac.uk

B. Azimi, E. Vasili, S. Danti
Department of Civil and Industrial Engineering
University of Pisa
Pisa 56126, Italy

D. A. Gregory, I. Roy
Insigneo Institute for in silico Medicine
University of Sheffield
Sheffield S102TN, UK

S. Linari
Linari Engineering s.r.l.
Pisa 56121, Italy

The ORCID identification number(s) for the author(s) of this article can be found under https://doi.org/10.1002/mame.202500074



**DOI: 10.1002/mame.202500074**

medium-chain length (MCL) PHAs containing six to thirteen carbon atoms in their monomeric units.[15] PHAs have gained attention in various biomedical applications, particularly in tissue engineering and the development of medical devices. SCL-PHAs, like poly(hydroxybutyrate) P(3HB), are known for their brittleness, stiffness, high crystallinity, low elongation at break, and high melting temperatures, and they are considered suitable for hard tissue engineering.[18–20] In contrast, MCL-PHAs are elastomeric, characterized by their high ductility, exhibiting over 300% elongation at break, and low glass transition temperature ($T_g$) (≈−35 °C or below), which is attributed to its MCL-alkyl side-chains and its copolymeric composition.[4,21] These properties render MCL-PHAs a well-suited choice for medical applications involving soft tissues or those in direct contact with the skin, such as wound dressings.[17,22,23] PHAs offer a wide range of desirable characteristics, including biocompatibility, excellent surface biodegradability profiles, the ability to modify mechanical properties to match specific tissue or organ properties, and cost-effective production from readily available carbon sources.[17] To mitigate the inherent brittleness of SCL-PHAs, several studies have blended them with specific amounts of MCL-PHAs. This approach aims to decrease the brittle nature of SCL-PHAs and render them better suited for various tissue engineering applications.[23,24]

Bacterial cellulose (BC) is a remarkable biomaterial produced by acetic acid-producing bacteria such as *Gluconacetobacter xylinus*. It is characterized by nanofibrils that are about a hundred times thinner than those found in plant cellulose.[25] Its high surface-area-to-volume ratio grants BC superb absorbent properties. It forms a porous crystalline polymer network that can transform into macrofibers, offering exceptional tensile strength and stiffness.[25,26] BC is intrinsically pure, requiring no extensive purification processes. It has diverse physical attributes, including high mechanical strength, high water-holding capacity, biocompatibility, nanostructure, and chemical stability, making it valuable in various applications, including tissue engineering, biomedicine, nanofluidics, wearable devices, functional foods, cosmeceuticals, and biocomposites.[26,27]

Despite recent progress in BC research, tissue engineering has yet to fully exploit the potential of BC as a material. Certain inherent drawbacks of BC, including irregular pore configuration and slow degradation or non-degradability, particularly under physiological conditions, are limiting factors in most tissue engineering applications. Therefore, significant attention has been directed toward modifying and fine-tuning the properties of BC to align with specific application requirements. One approach to achieve this is by reinforcing BC with other materials to create BC blends and composites, whether by in situ or ex situ modifications, where its intrinsic chemical, physical, and mechanical properties can be altered.[3]

Numerous studies have explored PHAs or blends and composites of their short-chain-length and medium-chain-length forms with various modifications, yielding electrospun fibers with enhanced physical and biological characteristics.[4,6,28–34] Similarly, research has been carried out to investigate pure BC nanofibers and their blends and composites with diverse materials.[35–39] Notably, the development of solution-based blends combining BC and PHAs for the fabrication of nano- or microfibers remains an unexplored innovation.

Hence, this study explored, for the first time, the novel approach of fabricating a blend material that combines BC and polyhydroxyalkanoates, both renewable and sustainable biocompatible polymers, each with their unique properties. An in-depth characterization of the materials was conducted to understand the chemical structure, surface properties, thermal properties, and finally the protein adsorption and cytocompatibility of the blends with respect to NG108-15 neuronal cells. The results obtained in this work, for the first time, indicate that the blends are highly suitable for nerve tissue engineering and possibly highly promising materials for other tissue engineering and controlled drug release applications.

## 2. Results and Discussion

### 2.1. Surface Morphology of the Electrospun Fibers by Scanning Electron Microscopy (SEM)

Electrospinning of BC resulted in the production of continuous, bead-free nanofibers, with an average diameter of 0.46 ± 0.13 µm (**Figure 1**A,D). Similarly, electrospinning a homogeneous solution of BC and PHA blend led to the formation of uniform nanofibers, with an average diameter of 0.74 ± 0.28 µm (Figure 1B,E). In contrast, when the PHA blend was electrospun alone, the resulting microfibers displayed a larger average diameter of 2.28 ± 0.45 µm (Figure 1C,F).

The SEM characterization in our current study revealed distinct fiber configurations with varying diameters for each material. This study differs from previous studies such as those carried out by Lizarraga-Valderrama *et al* (2019),[6] by exploring the potential use of these materials as the outer components of nerve guidance conduits (NGCs). Their cytocompatibility would be a significant advantage, and the porous fibrous network would allow the efficient exchange of nutrients and gases within the NGC microenvironment, thereby enhancing nerve regeneration. Hence, rather than individual, separate, and aligned fibers, we focused on creating a continuous sheet of fibers.

As the fiber density increased, the elastomeric MCL PHA-containing fibers tended to fuse during the rapid evaporation of the highly volatile chloroform as shown in Figure 1C. This fusion phenomenon was absent in the BC/PHA blend sample. It remains uncertain whether the utilization of the ionic solvent, 1-Butyl-3-methylimidazolium acetate (BMIMAc), instead of chloroform caused the prevention of this fusion, or if the chemical interaction between the polymers and other factors, such as physical proximity between the fibers, or solution concentration, contributed to this phenomenon. It is worth noting that a similar issue was reported by Kalaoglu-Altan et al. (2021) in their electrospinning of P(3HO-*co*-3HD), an MCL-PHA and P(3HB). In the same studies, the authors reported suboptimal results when employing ether-based solvents, leading to unfavorable outcomes with low-quality fiber depositions marked by wet and fused nanofibers and reduced porosity. Conversely, using fast-evaporating solvents like chloroform and dichloromethane produced a more porous nanofibrous membrane, although the fibers retained their fused state. The authors emphasized the importance of attaining an appropriate polymer concentration to prevent post-deposition fiber fusion induced by residual solvents. Careful consideration of the SCL/MCL-PHA ratio is es-

 

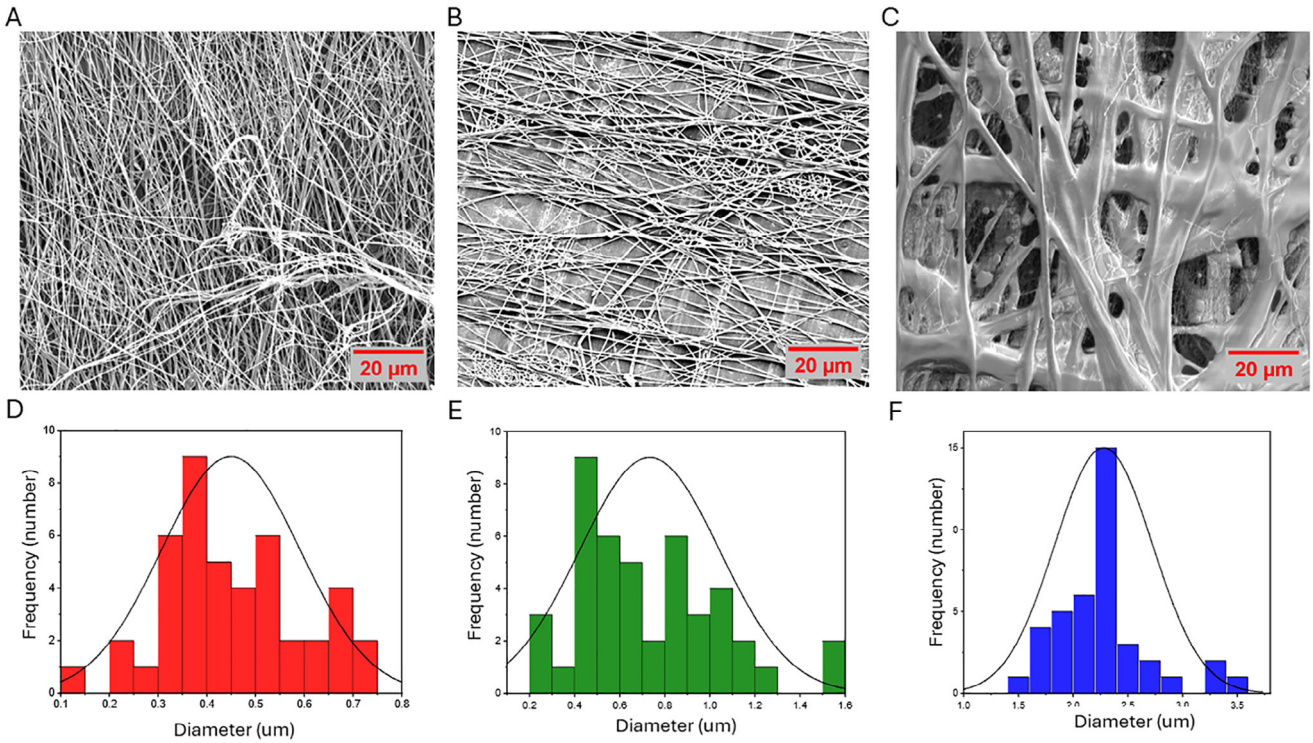


**Figure 1.** SEM images A) BC, B) BC/PHAs, and C) PHAs showing the morphology of the continuous electrospun fibers. Graph presenting the frequency distribution of fiber diameters observed in D) BC, E) BC/PHAs, and F) PHAs. Scale bar: 20 µm.

sential when electrospinning using the high evaporating solvent system. An excessive amount of SCL-PHA can result in the generation of brittle fibers and loss of elasticity, while an excess of MCL-PHA can lead to fibers fusion, especially in thicker membranes.[4]

The limited solubility of cellulose in both water and typical organic solvents poses a significant challenge for its application in electrospinning due to strong molecular stabilization through hydrogen bonds, electrostatic, and hydrophobic interactions within the fibrils.[36,40] However, several studies have explored the use of solvent systems containing ionic liquids to dissolve cellulose, such as N-methylmorpholine-N-oxide (NMMO), tetra(n-butyl) ammonium hydroxide (TBAH)/Dimethyl sulfoxide (DMSO), lithium chloride (LiCl)/dimethylacetamide (DMAc), (lithium hydroxide (LiOH)/urea, sodium hydroxide (NaOH)/urea, and 1-butyl-3-methylimidazolium formate (BMIMFmO).[36,72–76] It has also been well-documented that the modification of cellulose derivatives significantly enhances their solubility in common solvent systems. For instance, cellulose acetate, widely used in electrospinning, can be dissolved in solvents like acetic acid, acetone/DMAc, or acetone/DMF/water. High molecular weight hydroxypropyl methylcellulose resulted in homogeneous solutions in ethanol within the 1–6 w/w% concentration range. Consequently, the functionalization of cellulose plays a crucial role in the formulation of solutions suitable for electrospinning.[36,41–44]

Chloroform was used to dissolve neat PHAs, while a single solvent system (BMIMAc/DMSO) in a ratio of 1:3, respectively, was employed for both neat BC and BC PHA blends. This method was essential for achieving optimal fiber formation for each material, as chloroform is well-established for dissolving PHAs,[45,46] while BMIMAc/DMSO proved to be an effective solvent for BC. Although this choice of solvents may influence fiber morphology, the focus was on characterizing material composition, which is a key factor in cell interactions. The successful production of uniform sheets across all compositions indicates that the choice of solvent did not compromise scaffold's biocompatibility. Future research may explore solvent optimization for specific fiber morphology or enhanced structural control.

Unlike many DMSO-based systems that use co-solvents like tetrahydrofuran (THF) and dimethylformamide (DMF), where low miscibility with DMSO in certain polymer solutions can lead to phase separation and result in networked or bead-like fiber morphologies,[7] the DMSO/BMIMAc combination used in this study facilitated the formation of well-defined nanofibers. BMIMAc, an ionic liquid, enhances the solubility and uniformity of solutions containing cellulose and other polymers that are difficult to dissolve in common solvents.[47] This enhancement could be attributed to its ability to disrupt polymer chain interactions, particularly hydrogen bonding in polymers like BC, which rely heavily on these interactions for structural cohesion.[47,48] Consequently, BMIMAc promotes a more uniform polymer distribution, contributing to the stability of the electrospinning jet and minimizing bead formation and the development of network structures. Xu et al. (2008) demonstrated that incorporating DMSO into the 1-allyl-3-methylimidazolium chloride (AMIMCl) during the electrospinning of cellulose resulted in a significant reduction in solution viscosity, surface tension, and polymer network entanglement, alongside an increase in conductivity.[49] This combination fostered the formation of a sta-

ble electrospinning jet.[49] Given the structural similarities between AMIMCl and 1-butyl-3-methylimidazolium acetate (BMIMAc) as imidazolium-based ionic liquids, it is likely that the DMSO co-solvent used in our BMIMAc system produced comparable effects. These modifications in solution characteristics likely facilitated the controlled formation of fibers, thereby minimizing defects and enhancing fiber uniformity. Additionally, BMIMAc influences the rheological properties of the solution by modifying viscosity and surface tension, both critical factors for stable jet formation and fiber drawing.[48]

In the electrospinning process, the distance between the needle and the collector is a critical parameter, affecting the morphology, diameter, and uniformity of the produced nanofibers.[50,51] Generally, increasing this distance results in a reduction of fiber diameter due to the longer time available for solvent evaporation and the increased stretching of the polymer jet.[50,51] In contrast, shorter distances typically produce thicker fibers because insufficient solvent evaporation occurs before the fibers reach the collector.[50]

Moreover, the needle-to-collector distance influences the instability of the electrospinning jet, often referred to as "whipping," which plays a significant role in the uniformity of fiber diameter. At greater distances, the extended time for electrostatic interactions—such as electrostatic repulsion within the jet and attraction to the collector—enhances fiber alignment and promotes a more ordered nanofiber structure.[50,52] This alignment is particularly important for applications such as fabricating NGCs, where controlled fiber orientation provides essential cues for nerve regeneration. Conversely, shorter distances can lead to increased variability in fiber diameter and less ordered fiber orientation.[50] Additionally, the use of fast rotating mandrels can further facilitate the production of highly aligned nanofiber structures.[52]

### 2.2. Characterization of Electrospun Fibers using Atomic Force Microscopy

The evaluation of the electrospun fibers using Atomic Force Microscopy provided an understanding of their topography, surface roughness, and adhesion characteristics (**Figure 2**). Surface roughness, denoted by parameters average roughness ($R_a$) and Root mean square roughness ($R_q$), revealed variations between the samples. This analysis provides valuable insights into the nanoscale properties of these polymers, crucial for cellular interactions.

BC fiber surfaces exhibited the lowest surface roughness ($R_a$ = 3.27 nm, $R_q$ = 4.82 nm), confirming their smooth surface characteristics seen in SEM. The BC/PHA blend exhibited intermediate roughness ($R_a$ = 10.6 nm, $R_q$ = 14.2 nm,). As expected, the PHA blend had the highest roughness ($R_a$ = 64.4 nm, $R_q$ = 79.7 nm), likely due to the presence of hydrophobic regions within the MCL-PHAs.

Additionally, the study investigated the adhesion forces between the samples and the hydrophobic AFM tip. BC had the lowest adhesion (average force = 3.3 nN), indicating moderate adhesive properties with a small spread in the data. The BC/PHA blend displayed intermediate adhesion (average force = 12.2 nN), suggesting a stronger interaction with the AFM tip. Critically it was clear that the data was so much spread most likely due to the immiscible blend of SCL and MCL PHAs combined with BC and indicated potential regions of phase separation. The PHA blend showed the highest adhesion (average force = 30.5 nN), indicating the strongest adhesive characteristics. The adhesion characteristics provide insights into the hydrophobic and hydrophilic nature of the polymer surface, with stronger adhesion to the AFM tip generally indicating greater hydrophobicity in that region.[53] It is important to note, however, that stronger adhesion to the AFM tip does not directly correlate with reduced cell attachment, as such a conclusion would require measurements using a cell-attached AFM tip. Nonetheless, when considered alongside surface roughness data, the adhesion behavior appears to offer strong indicative trends.

The higher surface roughness together with adhesive properties might enable better cell attachment.[53,54] These results correlate to the smooth surface and low adhesion of cells observed in the highly hydrophilic BC sample.[3] The BC/PHA blend, with increased roughness due to PHA presence most likely due to the SCL content, exhibited proportionally enhanced adhesion compared to the BC-only sample.

### 2.3. Differential Scanning Calorimetry (DSC)

DSC analysis was conducted to explore the thermal behavior of the polymeric fibers. In the PHA blend sample (50:50 (w/w %) P(3HB)/MCL-PHAs blend), two distinct melting temperatures ($T_m$) were observed at 49.35 °C ($T_{m1}$) and 165.39 °C ($T_{m2}$) attributed to the presence of the two distinct components, MCL PHAs and P(3HB), respectively. The small endothermic peak observed at 49.35 °C ($T_{m1}$) suggests a complex interaction between the two polymers. According to the literature, this peak may indicate the presence of a rigid amorphous fraction (RAF) in the P(3HB) component,[55] although the melting behavior of the MCL-PHA component is more likely to be the main contributor due to its significant proportion (50 w%). MCL-PHAs typically have a melting temperature of around 50 °C.[56] However, the presence of P(3HB), which exhibits distinct crystallization behavior (Tc of ≈50 °C upward),[55] could influence the crystallization of MCL-PHA. This interaction could result in less perfect crystallites or a change in the overall crystallinity of the MCL-PHA component, leading to a smaller and potentially broader melting peak. At $T_{m2}$, representing the melting temperature of P(3HB), two distinct crystalline phases were observed in the sample, each displaying its melting temperature, as depicted in Figure 4, hence the presence of two peaks. The BC sample, on the other hand, exhibited an endothermic peak at 97.06 °C. Although George et al. (2005) have associated endothermic peaks occurring at (≈120 °C) with the crystalline melting temperature of cellulose, and a glass transition around 13.94 °C,[58] the peak observed in this study, at ≈100 °C, is more likely to be attributed to the evaporation of water trapped within the BC structure. This phenomenon is commonly observed in cellulosic materials, and the relatively low thermal event further supports this interpretation.[57] However, the peak observed at 17.33°C possibly represents the glass transition temperature ($T_g$) of BC.[58,59]

Finally, the BC/PHA blend exhibited a broad endothermic peak at ≈97.06 °C during DSC analysis. This peak is consis-

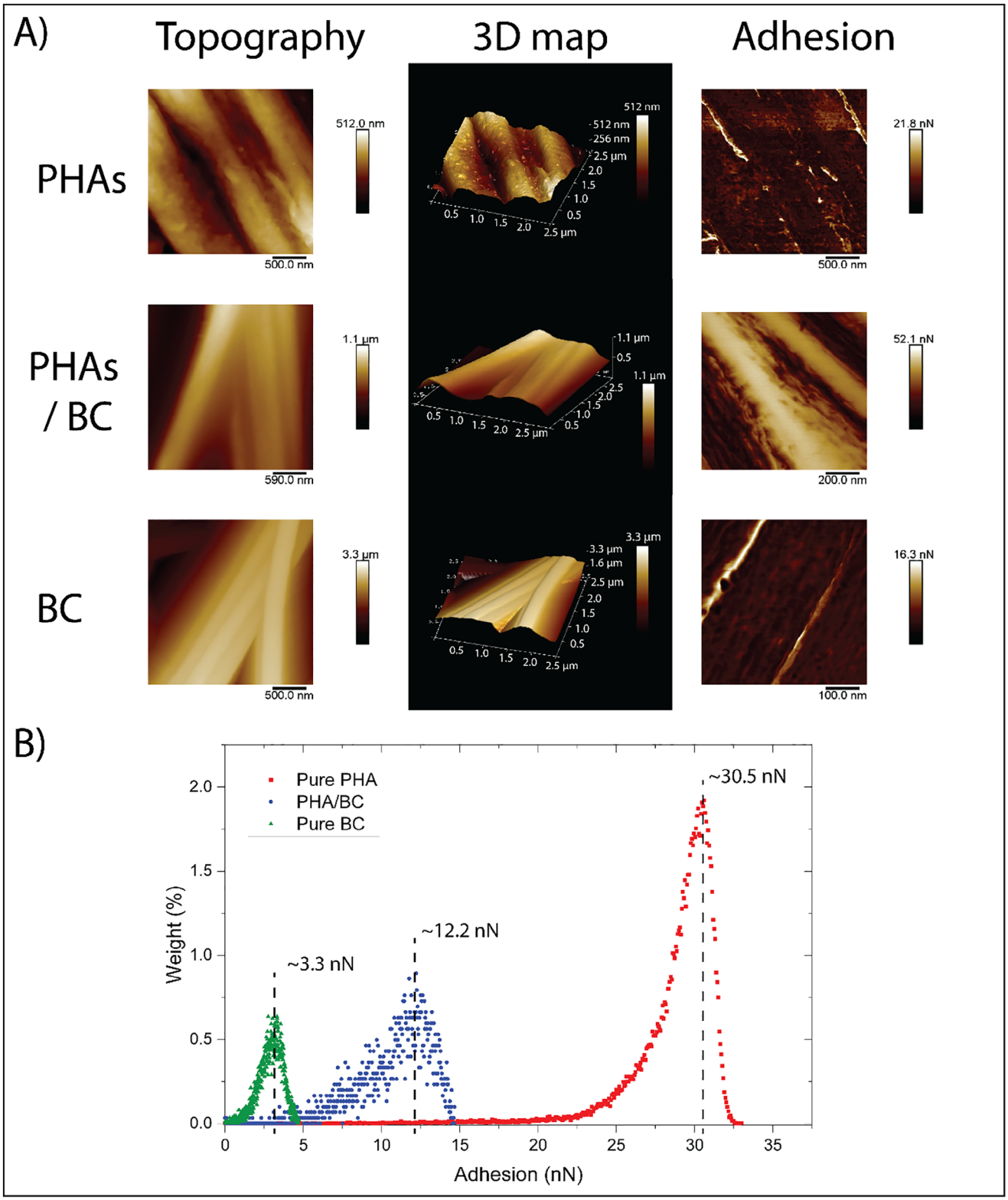


**Figure 2.** A) Representative Atomic Force Microscopy surface topography micrographs including 3D renderings and adhesion maps. B) Adhesion distribution histograms for Pure PHA (blend), PHA (blend)/BC, and Pure BC fibers samples, the adhesion indicates the adhesion properties of the hydrophobic AFM tip to the polymer surface.

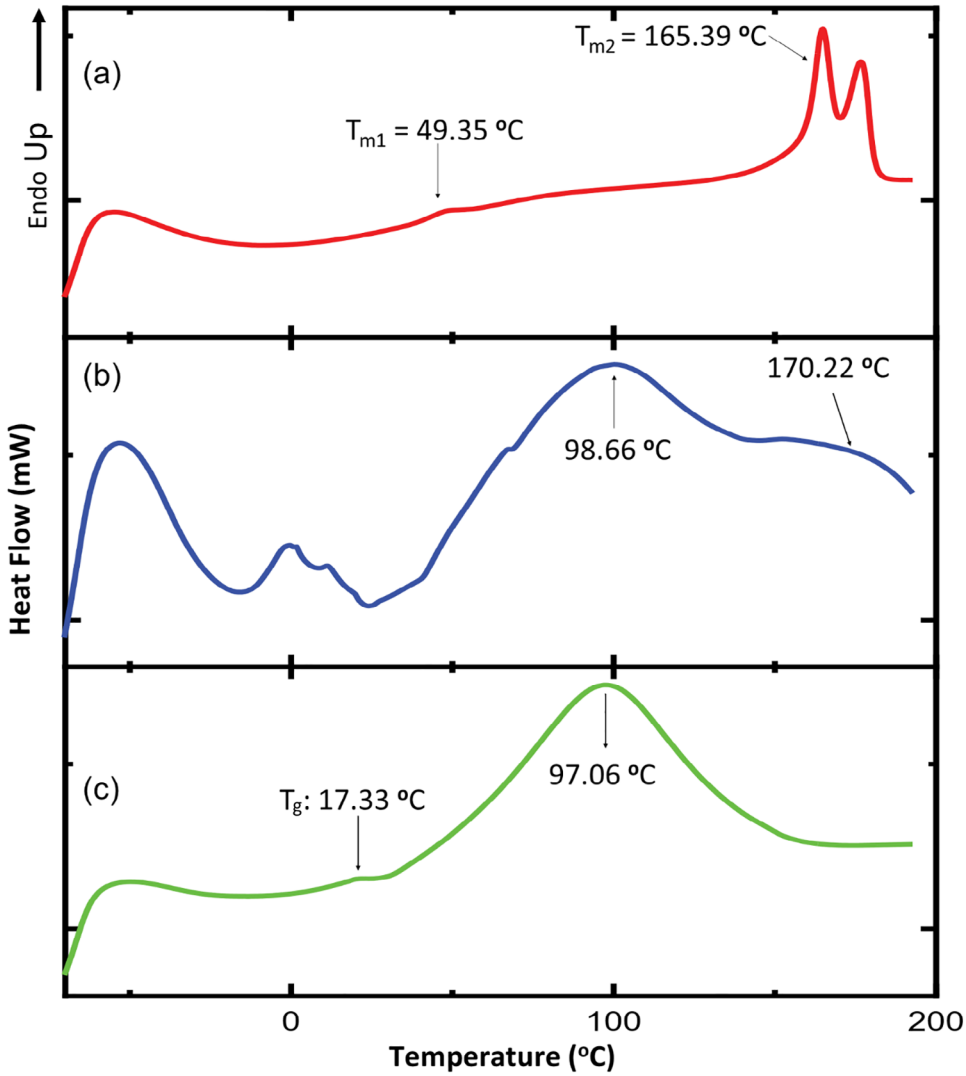


**Figure 3.** Thermal properties of the electrospun fibers a) Blend PHAs b) BC/PHA, and c) BC obtained under − 70 °C and 200 °C heating conditions at a rate of 20 °C $min^{-1}$.

tent with the observed water evaporation peak in pure BC. The absence of a specific $T_m$ for the PHAs within the blend indicates the possibility of interactions between BC and the PHAs. These interactions may obscure the individual $T_m$ of the PHA components, as illustrated in **Figure 3**. Moreover, the DSC thermogram of the BC/PHA blend displayed several small peaks near 0 °C, which were not present in the pure polymers. These peaks may arise from the formation of new localized environments or phases due to interactions between BC, PHB, and MCL-PHA. These components may undergo thermal transitions near 0 °C. The broad peak observed around 170.22 °C likely signifies a distinct melting behavior that differs from the behavior of the individual polymers. The broadness of this peak suggests a range of crystallite sizes and degrees of crystallinity within the blend, which may be influenced by BC's effect on PHA crystallization. Alternatively, this peak may be attributed to interactions or cross-linking between the components during blending. These interactions could alter the thermal properties of the blend and result in a less well-defined melting process.

Thermal analysis revealed endothermic peaks around 100 °C for both BC and the BC/PHA blend. These peaks can be attributed to the evaporation of water trapped within the BC matrix. The amorphous MCL-PHA component of the blend showed a melting temperature of ≈50 °C. In contrast, the highly crystalline P(3HB) demonstrated a distinct double-peak near 170 °C, indicating the presence of well-defined crystalline domains and suggesting an immiscible blend.

### 2.4. Thermogravimetric Analysis

Thermogravimetric analysis (see **Figure 4**) was also conducted to assess the thermal stability and degradation characteristics of the electrospun fibers. For BC, TGA revealed a characteristic thermal profile, with a substantial proportion of its weight loss occurring

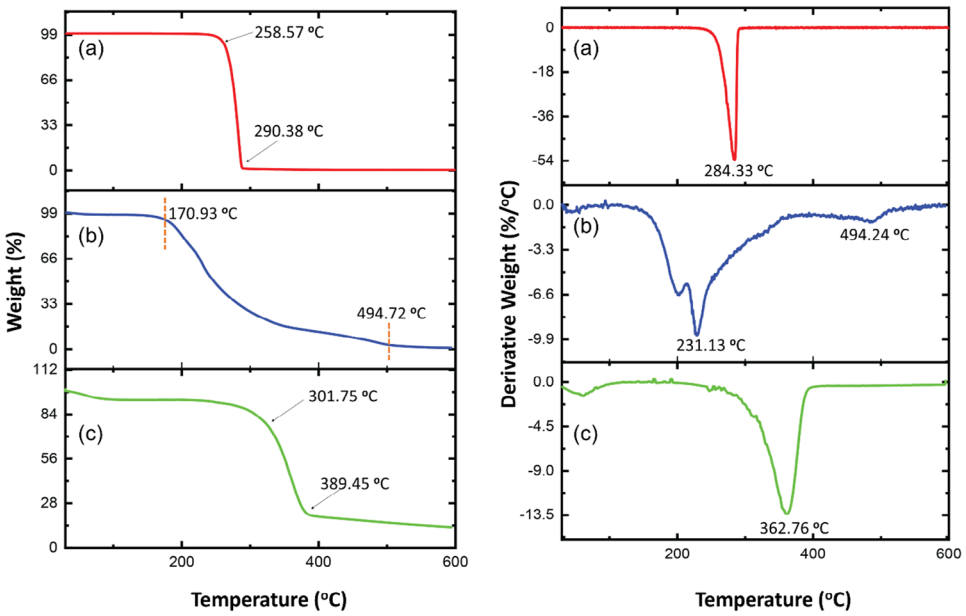


**Figure 4.** TGA of the electrospun fibers weight % (left) and weight derivative % cycle (right). a) Blend PHAs b) BC/PHAs c) BC.

at ≈360 °C, in line with the expected behavior of cellulose materials. The PHA sample displayed a distinct thermal profile, featuring a complete weight loss at 290 °C. In the case of the BC/PHA blend, TGA revealed a deviation from the thermal characteristics observed in the individual components. A distinct thermal degradation was observed in one component of the blend at ≈231.13 °C, indicating a lower decomposition temperature compared to the neat BC and PHA blends. Additionally, another component of the BC/PHA blend exhibited degradation at 494.24 °C, which is significantly higher than the corresponding temperature observed in the neat polymers.

The thermal degradation behavior of the PHA blends analyzed in this study was found to be lower than the decomposition temperatures observed by Lukasiewicz et al., which were within the range of 350–370 °C.[59] The results obtained show the unique behavior of the blended sample, suggesting a strong interaction between the BC and PHA components in the blend. Additionally, George et al. (2005) reported a degradation temperature of 298.07 °C for native cellulose, while NaOH-treated BC demonstrated enhanced thermal stability with a degradation temperature of 343.27 °C.[58]

### 2.5. Protein Adsorption by the Electrospun Fibers

The protein adsorption capacity of the electrospun fibers, namely BC, BC/PHA, and PHAs was investigated (**Figure 5**). The BC/PHA blend exhibited a slightly higher protein adsorption capacity (404 μg $cm^{-2}$) than neat BC (396 μg $cm^{-2}$) and PHA blends (370 μg $cm^{-2}$). However, these differences were not statistically significant ($p > 0.05$), indicating comparable protein-binding affinities across all three materials. While protein adsorption remained similar, the BC/PHA blend demonstrated marginally improved cytocompatibility, suggesting that blending BC with PHA modulates surface characteristics influencing cellular interactions. As has been previously shown, cell adhesion is strongly dependent on the presence of specific protein-binding sites.[60] The observed improvement in cell adhesion likely results from the interplay between BC's hydrophilic nature and PHA's hydrophobic domains, creating a chemically diverse interface with tailored surface roughness that promotes better integrin-mediated cell attachment. These findings suggest that the BC/PHA blend provides a more favorable substrate for cell adhesion, potentially enhancing overall biocompatibility.

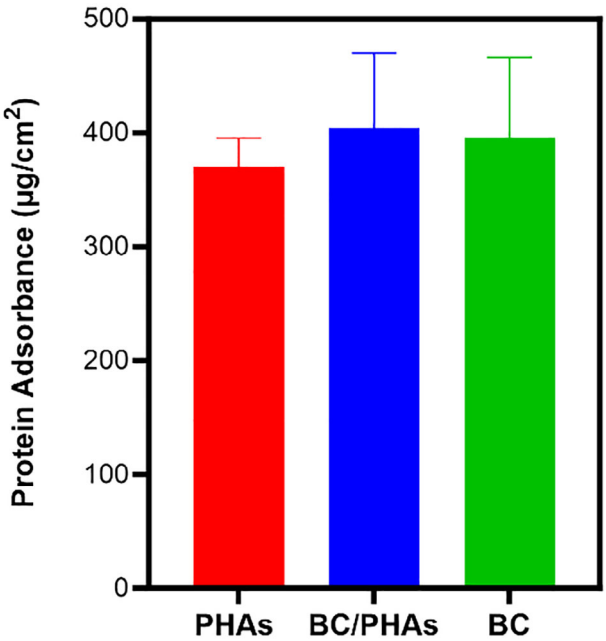


**Figure 5.** Protein adsorption assay. The graph shows the results of protein adsorption studies on the electrospun fibers, i.e., BC, the blend of BC and polyhydroxyalkanoates and the polyhydroxyalkanoate blend.

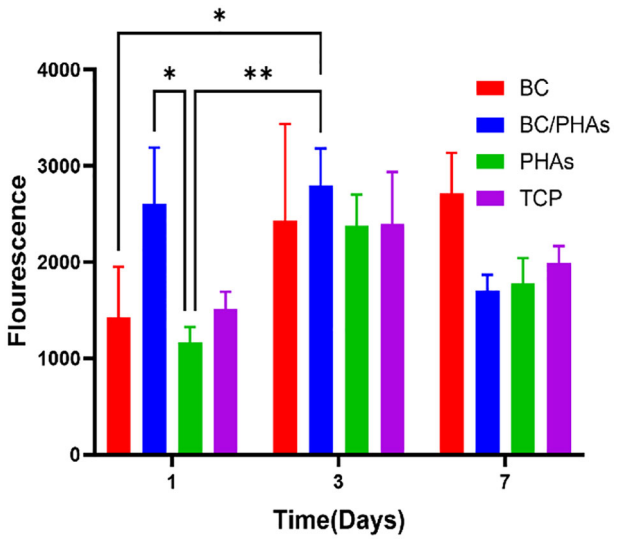


**Figure 6.** Cell viability (Resazurin fluorescence) of NG108-15 neuronal cells cultured on individual electrospun fiber substrates and TCP. Cell viability was determined at 1, 3, and 7 days. A two-way ANOVA with Tukey's multiple comparison tests was used to analyse the data (mean ± SD, $n$ = 3 independent experiments *$p < 0.05$, **$p < 0.01$, ***$p < 0.001$ and ****$p < 0.001$).

### 2.6. Metabolic Activity of NG108-15 Cells on the Electrospun Fibers

The Resazurin assay was conducted to assess the metabolic activity of cells on the different electrospun fibers over seven days (**Figure 6**). The fluorescence measurements and their corresponding standard deviations provide insights into cellular metabolic responses: On Day 1, BC exhibited a higher metabolic activity (1427.11 ± 522.6) as compared to PHAs (1 167.33 ± 156.82) and was slightly lower than the TCP control (1 507.22 ± 186.3). Remarkably, BC/PHA exhibited the highest metabolic activity among the materials on Day 1, exhibiting a fluorescence measurement of 2 604.0 ± 583.76, which demonstrated a low, yet statistically significant difference compared to the PHA sample. As the experiment progressed to day 3, BC (2 433.22 ± 1 003.34) displayed slightly higher metabolic activity compared to the PHA blend (2 377.9 ± 323.61) and the TCP control (2 397.22 ± 539.44), while BC/PHA (2 792.56 ± 385.84) continued to demonstrate the highest metabolic activity among the materials. By Day 7, BC (2 717.67 ± 418.27) showed the highest metabolic activity among the materials, followed by the TCP control (1 995 ± 171.98), BC/PHA blend (1 701.79 ± 167.24), and the PHA blend (1 777.78 ± 267.22). However, there was no statistical difference among the samples.

### 2.7. Live/Dead Assessment of NG108-15 Neuronal Cells on Electrospun Fibers

The Live/Dead assay was conducted to assess the cell viability on different electrospun fibers after a seven-day culture period (**Figure 7**). The cell populations, represented by live cells, are summarized as follows, with mean values and standard deviations: On Day 7, BC fibers demonstrated a cell population of 117.78 ± 69.62 of live cells, while bacterial BC/PHAs fibers supported 143.1 ± 24.62 live cells. The PHA blend fibers supported 90.56 ± 16.41 live cells, and the TCP control supported 209 ± 26.55 live cells.

### 2.8. Assessment of Neurite Outgrowth of NG108-15 Neuronal Cells on the Electrospun Fibers

In the assessment of neurite outgrowth, the electrospun fibers displayed varying average neurite lengths, as shown in (**Figure 8A–D**). The BC fiber substrate exhibited an average neurite length of 182 ± 12.93 µm. BC/PHA displayed a slightly longer average neurite length of 187.9 ± 4.35 µm, the PHA blends showed a slightly shorter average neurite length of 162.57 ± 13.07 µm (Figure 8E). The Tissue Culture Plastic (TCP) control had an average neurite length of 152.74 ± 33.9 µm. Comparatively, BC/PHA exhibited the longest average neurite length among the electrospun fibers, while PHA blend, and TCP displayed slightly shorter average neurite lengths. Furthermore, assessing the maximum neurite lengths, the electrospun fibers exhibited varying capabilities: BC supported a maximum neurite length of 254.63 ± 31.92 µm and BC/PHA blend demonstrated the longest maximum neurite length of 273.3 ± 36.21 µm. The PHA blend displayed a maximum neurite length of 250.65 ± 29.8 µm. The TCP control exhibited a maximum neurite length of 207.58 ± 41.4 µm (Figure 8F).

BC is valued for its exceptional mechanical properties and inherent biocompatibility, which guided the decision to blend it with PHAs. Its nanofibrillar architecture closely resembles the extracellular matrix of native tissues, creating a favorable environment for cell attachment, proliferation, and neurite extension, qualities essential for tissue regeneration.[27,28,71] The combination of this nanofibrillar structure and hydrophilic nature may enhance protein adsorption and cell adhesion. Blending BC with hydrophobic PHAs results in a tunable material with controlled degradation and mechanical flexibility, making it suitable for neural applications. The thermal stability provided by BC, as demonstrated in this study, is crucial for maintaining material integrity during processing and sterilization, both of which are vital for biomedical applications. Additionally, its high water absorbency supports nutrient diffusion and cellular viability within nerve regeneration scaffolds, creating an optimal microenvironment for Schwann cell survival and axonal growth, factors that promote successful nerve repair.[61]

For biological activity, in our current investigations, the BC/PHA sample displayed the highest cell metabolic activity until day 3 of cell culturing. However, by day 7, the pure BC sample showed slightly higher metabolic activity, although this difference was not statistically significant. This variation could be attributed to potential over-proliferation leading to reduced cellular activity in the BC/PHA sample, as evidenced by the Live/Dead analysis. The BC/PHA blend also resulted in the longest average and maximum neurite length, implying its ability to support extensive neural cell development. In summary, our cytocompatibility assessment, which included evaluations of cell metabolic activity, cell viability, and neurite extensions, demonstrated that the BC and PHA blend exhibited superior cytocompatibility, sug-

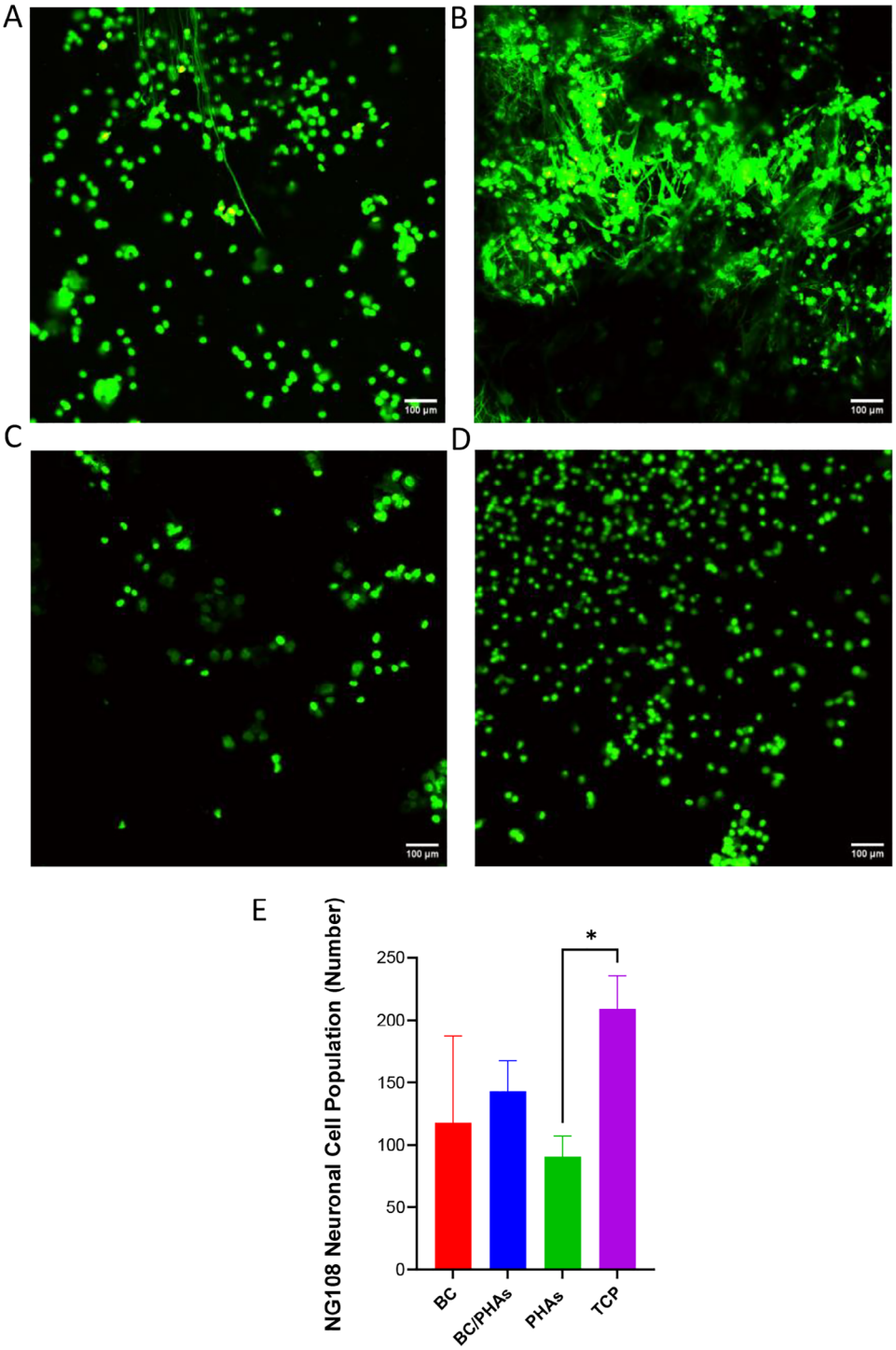


**Figure 7.** Confocal micrographs of NG108-15 neuronal cells cultured on A) BC fibers, B) BC/PHA fibers, C) PHA blend fibers, and D) TCP. E) Graph showing the cell populations that were alive on the fiber substrates on Day 7 of cell culture. Scale bar = 100 µm.

gesting that the BC/PHA blend provides a more conducive environment for robust neural cell interactions and activity.

While we did not directly measure tensile strength in this study, BC is recognized for enhancing the mechanical properties of polymer matrices. The successful electrospinning of the BC/PHA blend into uniform nanofibrous scaffolds that incorporated the unique features of both polymers may indicate improved structural integrity and compliance; it is also possible that the electrospinning process itself further enhanced the blend's mechanical properties. Our primary focus in this study was to

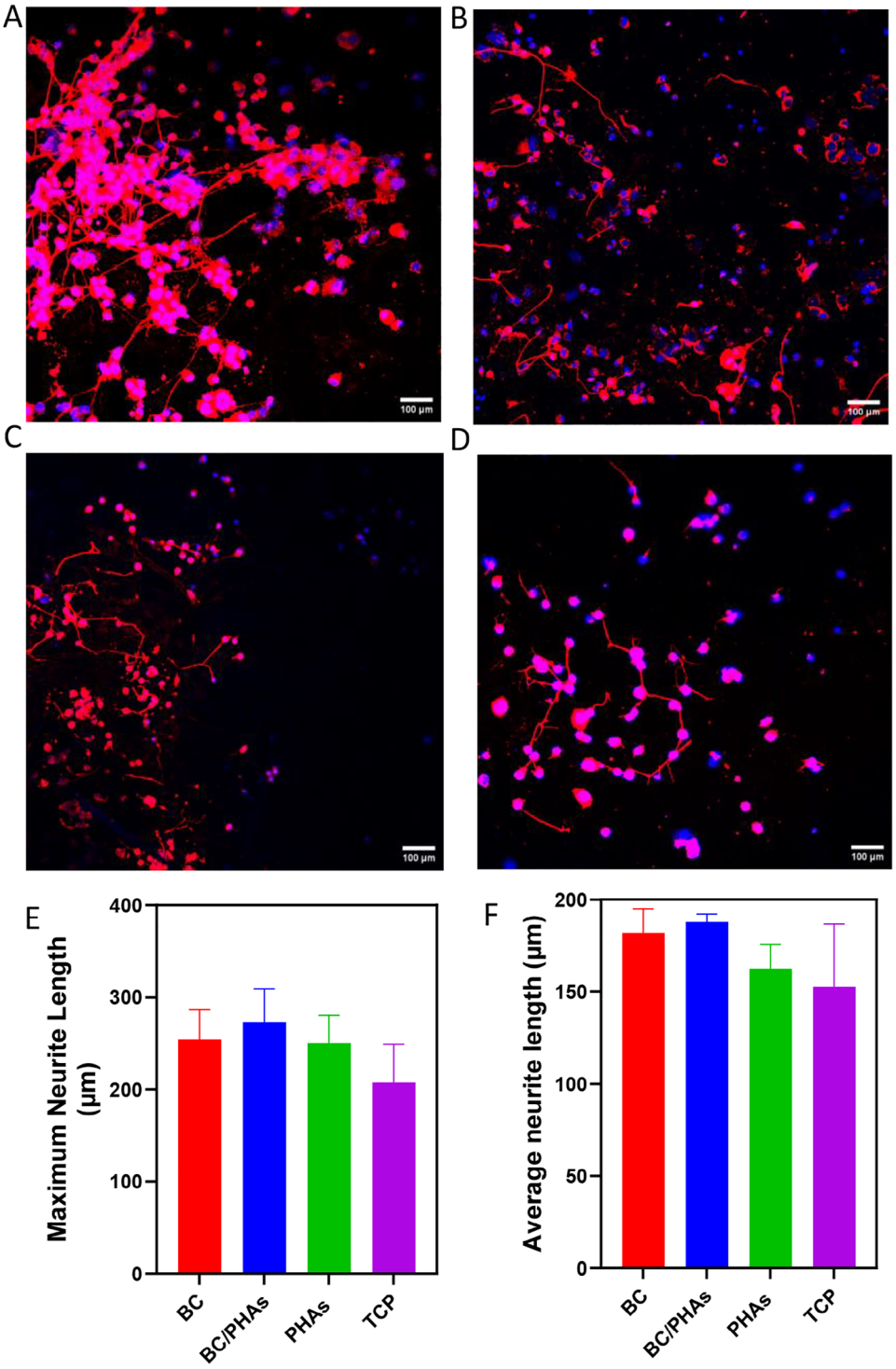


**Figure 8.** Confocal microscopy images of NG108-15 neuronal cells immunolabeled using $\beta$ III tubulin (red) and cell nuclei (blue). Cells were stained after 7 days in culture on A) BC fibers, B) BC/PHA fibers, C) PHA fibers, and D) TCP. E) Graph showing the maximum neurite length achieved by the individual samples. F) Graph showing the average neurite length achieved by the individual samples. Scale bar = 100 µm.

establish the material's biological compatibility and viability as a scaffold. In addition to these, given BC's limited degradation in vivo, blending it with biodegradable PHAs may enable controlled resorption. The degradation of PHAs can break down the BC network, facilitating its eventual clearance. Future research will, therefore, investigate methods to modify BC, such as oxidation and cellulase pretreatment, to enhance its degradation in vivo and study direct mechanical testing to quantify these improvements.

## 3. Conclusions

In conclusion, this study highlights the potential of blends composed of BC and PHAs for applications in nerve tissue engineering. This study successfully produced uniform and bead-free nanofibers from pure BC and a BC/PHA blend using electrospinning. The fiber diameters varied with composition: BC yielded the thinnest nanofibers (≈0.46 µm), followed by the BC/PHA blend (≈0.74 µm), and neat PHAs generated the thickest microfibers (≈2.28 µm). Also, morphological studies have shown a distinct pattern in surface roughness. BC exhibited the smoothest surface, PHA had the roughest surface, and the BC/PHA blend displayed intermediate roughness. This observation aligned with the adhesion forces, which increased with surface roughness, likely due to hydrophobic interactions. Thermal analysis indicates that BC fibers possess excellent thermal stability, with degradation primarily occurring around 360 °C, which is consistent with the behavior of cellulose. PHA displayed complete weight loss at 290 °C. Interestingly, the BC/PHA blend exhibited altered thermal degradation behavior compared to its components, showing distinct degradation stages at 230 and 490°C. This suggests potential interactions between BC and PHA within the blend that influence their thermal stability. Our findings indicate that BC/PHA blends show a trend toward improved cell viability and neurite outgrowth in NG108-15 neuronal cells, suggesting potential advantages over neat BC and PHA for nerve repair applications, thus warranting further investigation. In addition to tissue engineering, BC/PHA blends have the potential for broader applications, such as drug delivery and various bulk applications. They offer a compelling alternative to existing materials by effectively combining the advantageous characteristics of two natural materials. This study emphasizes the importance of exploring novel material combinations and the crucial role of natural materials in advancing the fields of regenerative medicine and biomedical engineering. Future research will focus on investigating the capabilities of these materials in producing 3D nerve guidance scaffolds and conducting in vivo studies to evaluate their full clinical potential.

## 4. Experimental Section

*Materials*: Both BC and PHAs were synthesized using the methods described in the references[62] for BC,[63] for medium chain length PHAs (MCL-PHAs), and[64] for short chain length PHAs (SCL-PHAs) or P(3HB), in the laboratory of Professor Ipsita Roy at the University of Sheffield, United Kingdom. The two types of PHAs were used to create a blend of equal parts: MCL and SCL- PHAs, i.e., a 50:50 w% blend.

*Fabrication of Electrospun Fibers*: Electrospun fibers were produced using three different conditions for comparative analysis: pure BC, a blend of Short-Chain-Length and Medium-Chain-Length Polyhydroxyalkanoates, and a solution of BC and the blended PHA. The electrospinning solutions were prepared and optimized as follows: for BC, a method described previously[65–67] was followed. A 3 w% BC solution was created by dissolving BC in 1:3 proportions of 1-Butyl-3-methylimidazolium acetate and Dimethyl Sulfoxide and electrospun under specific conditions (**Table 1**). For PHAs, a 10 w% PHA solution was made by dissolving equal amounts of SCL and MCL-PHA in chloroform and electrospun. Last, a blend solution containing 2 w% BC, 2 w% SCL-PHA, and 2 w% MCL-PHA (6 w% in total) was formulated, employing 1:3 proportions of BMIMAc/ DMSO and electrospun under specific conditions. SEM was used to analyze the morphology and diameter of the electrospun fibers for each condition.

*Fibers Morphological Characterization by SEM*: To assess the morphology of the electrospun fibers, samples were examined via SEM. Prior to SEM, the fibers were prepared and affixed to SEM stubs. A 20 nm gold layer was sputter-coated onto the fibers' surfaces to optimize surface conductivity and mitigate sample charging during imaging. High-resolution SEM analysis was conducted using an FEI Inspect F scanning electron microscope, which examined the fibers' microstructure. The resulting SEM images were visually inspected, and fiber diameters were analyzed using ImageJ (Version 1.54f; NIH, USA). For each group, 70 to 100 fibers were measured to assess variation.

*Fibers Topology Characterization by Atomic Force Microscopy (AFM)*: In tapping mode, surface roughness analysis of electrospun fibers was conducted using Atomic Force Microscopy (AFM). The study utilized SCANASYST-AIR probes on a Bruker Dimension Icon AFM, with the electrospun fibers placed on cover glass affixed to a magnetic AFM support. Characterization, including surface roughness ($R_q$, $R_a$), adhesion maps, and bearing analysis, was performed using Bruker's NanoScope Analysis software (Version 2.0). The study aimed to assess the electrospun fibers samples' adhesive properties using the SCANASYST-AIR probes. This AFM analysis, in conjunction with Bruker's advanced software, provided detailed insights into the microstructure and adhesive behavior of the electrospun fibers.

*Thermal Characterization of the Polymers by DSC*: The thermal characteristics, including the glass transition temperature ($T_g$) and melting temperature ($T_m$), of the electrospun fibers were examined through DSC, employing a Perkin Elmer DSC4000 apparatus with Pyris software. The analyses were performed in a nitrogen environment to prevent oxidation and ensure precise thermal assessment. The samples underwent two heating and cooling cycles at 20 °C/min, covering a temperature range from − 70 to 200 °C.

*Fibers Thermal Stability and Decomposition Studies by Thermogravimetric Analysis (TGA)*: The thermal stability and decomposition of the electrospun fibers were evaluated by thermogravimetric analysis (TGA) using a Perkin Elmer Pyris 1 TGA instrument. The analysis was conducted within a controlled nitrogen environment to safeguard against sample oxidation and ensure the precision of thermal measurements. The samples were heated at 10 °C/min, from 30 to 600 °C.

*Protein Adsorption Assay*: The protein adsorption assay aimed to quantitatively evaluate the total protein adsorption using undiluted fetal bovine serum (FBS) onto the solvent-cast films, following a well-established protocol.[12] Circular films, each covering an area of 4 $mm^2$, were meticulously arranged in a 24-well plate and immersed in 400 µL of undiluted FBS at 37 °C for 24 h. Subsequently, the films underwent three washing cycles using PBS and were transferred to a fresh 24-well plate. In the next step, the films were incubated in 1 mL of 2% (w/v) sodium dodecyl sulphate (SDS) in PBS, with gentle shaking, at room temperature for 24 h. The quantification of adsorbed proteins was conducted using the Bicinchoninic Acid (BCA) assay, and absorbance readings were taken at 562 nm with a spectrophotometer (Bio-Tek ELx 800 absorbance microplate reader).

*In Vitro Cell Culture with NG108-15 Neuronal Cells*: Sheets of fibers, each with ≈12 mm diameter, were securely affixed individually to 16 mm cover glasses with a sealant (King British Aquarium), and each was placed into an individual well of 12-well plates. To sterilize the samples, they were submerged in 70% ethanol/water solution for 1 h, followed by a thorough triple rinse, with each wash lasting 5 min and using sterilized PBS. The samples were subsequently immersed in PBS and placed within a Class

**Table 1.** Summary of electrospinning conditions.

| Solution | Concentration [w/w %] | Flow rate [mL0/h] | Rotor speed [rpm] | Distance [cm] | Voltage [kV] |
|---|---|---|---|---|---|
| BC | 3 | 0.5 | 50 | 10 | 23 |
| BC/PHA | 6 | 1 | 50 | 10 | 18 |
| PHAs | 10 | 1 | 50 | 10 | 18 |

II safety cabinet overnight. This process ensured the complete removal of any residual contaminants or solvents before introducing cells for seeding.

NG108-15 neuronal cells were sourced from frozen stocks and expanded to passage 15 for use in this experiment. The cells were cultured in Dulbecco's Modified Eagle Medium (DMEM) supplemented with 1% (w/v) penicillin/streptomycin, 10% (v/v) fetal calf serum, 0.5% (w/v) amphotericin B, and 1% (w/v) glutamine. Incubation was maintained in a humidified incubator at 37 °C with 5% $CO_2$ when cells reached a confluence of 90% or more using a trypsin/EDTA solution. For the cell culture, 12-well plates containing 2 mL of DMEM were seeded with 15 000 cells each and incubated at 37 °C as previously described. After 48 h of incubation, the culture medium in the wells was replaced with 1 mL of serum-free DMEM containing 1% (w/v) penicillin/streptomycin, 1% (w/v) glutamine, and 0.5% (w/v) amphotericin B.

*Cell Metabolic Activity Analysis*: The resazurin assay, which measures cellular metabolic activity, was employed to evaluate the viability of cells cultured on the film samples at 1-, 3-, and 7 days post-seeding. For each experiment, serum-free DMEM culture medium was aspirated from the cultured samples and washed with PBS. Fresh DMEM medium, combined with the resazurin reagent (constituting 10% of the total mixed volume) (Brand, city, country), was then added to the samples and incubated in a light-protected, humidified environment at 37 °C with 5% $CO_2$ for 4 h. Following incubation, triplicate samples ($n = 3$) from each well plate were transferred to a 96-well plate for analysis. The solution's fluorescence was measured at 450 nm using a fluorescence spectrophotometer (Brand, city, country).

*Cell Viability Analysis*: The viability of cells after 6 days of cultivation was evaluated using a previously described method.[68,69] Initially, the culture medium was replaced with fresh serum-free DMEM, which was supplemented with 0.1% (w/v) Syto-9 (Invitrogen,) and 0.15% (w/v) propidium iodide (Invitrogen). The cells were then incubated in a light-free, humidified incubator at 37 °C with 5% $CO_2$ for 30 min. Following incubation, the cell samples underwent a thorough triple wash with PBS. Subsequently, these samples were immersed in PBS for imaging. The imaging process was conducted using a Nikon A1 laser scanning confocal microscope (Nikon). The fluorescence of propidium iodide ($\lambda_{ex}$ = 536 nm/$\lambda_{em}$ = 617 nm) was excited with a helium–neon laser, while Syto 9 fluorescence ($\lambda_{ex}$ = 494 nm / $\lambda_{em}$ = 515 nm) was induced by an argon-ion laser. This experiment was carried out in triplicate for each sample type and repeated three times to ensure consistency and reliability.

*Evaluation of Neurite Sprouting*: The assessment of neurite sprouting in NG108-15 cells was carried out utilizing $\beta$III-tubulin as the primary antibody and Texas Red-conjugated anti-mouse IgG as the secondary antibody, following established procedures.[70] The quantitative evaluation of neuronal differentiation was based on two key parameters: neurite length and the maximum neurite length. After a 6-day incubation, the culture medium was removed, and the samples underwent a series of treatments. This included fixation with 3.7% paraformaldehyde (w/v) (Sigma, United Kingdom) for 20 min, permeabilization with 1% Triton X-100 (v/v) (Fisher Scientific, United Kingdom for 30–45 min, and a thorough triple wash with PBS. A 30-min incubation with 3% bovine serum albumin (BSA) (w/w) (Fisher Scientific, United Kingdom) was performed to minimize nonspecific binding. Subsequently, the samples were exposed to a 48-h incubation at 4 °C with mouse anti-$\beta$III-tubulin antibody (Promega, USA) at a concentration of 0.2% in 1% BSA (w/w), followed by incubation with Texas Red-conjugated anti-mouse IgG antibody at 0.4%, and staining with 4',6-diamidino-2-phenylindole dihydrochloride (DAPI) at 0.2% at room temperature for 3 h. For imaging, a Nikon A1 laser scanning confocal microscope was employed with laser excitation and emission sources for Texas Red ($\lambda_{ex}$ = 589 nm / $\lambda_{em}$ = 615 nm) and DAPI ($\lambda_{ex}$ = 358 nm / $\lambda$em = 461 nm). Neurites within each visual field were manually traced using ImageJ (Version 1.54f; NIH, USA) from the soma to the distal end of each neurite. Only neurites that originated from the soma and had a clear endpoint were included for analysis. The experiment was carried out in triplicate for each type of sample and repeated three times.

*Statistical Analysis*: Data collected in this study underwent comprehensive analysis using GraphPad Prism software (GraphPad Software, USA). A one-way analysis of variance (ANOVA) with a significance level set at $p < 0.05$ was employed to assess the differences between datasets and determine their statistical significance. Additionally, paired Student's *t*-tests were utilized as appropriate. It is essential to note that each experiment was independently conducted thrice, and this is represented as $n = 3$ for statistical validity.

## Acknowledgements

The authors acknowledge all the partners involved in this project. This project has received funding from the European Union's Horizon 2020 research and innovation programme H2020-MSCA-RISE under grant agreement No. 777926, and the authors thank Professor Gwendolen Reily who was the main PI for this project and agreed to fund this mobility visit by E.A. E.A. and D.A.G. were also funded by ECOFUNCO (Grant Agreement No. 837863). I.R. was funded by the EPSRC grants EP/X026108/1, EP/V012126/1, and EP/X024040/1. C.S.T. was funded by the School of Chemical, Materials and Biological Engineering. University of Sheffield. S.D., E.V. and B.A. also acknowledge the fund from the Italian Ministry of University and Research (MUR) as part of the PON 2014-2020 "Research and Innovation" resources-Green/Innovation Action-DM-MUR 1061/2021.

## Conflict of Interest

The authors declare no conflict of interest.

## Author Contributions

E.A. was responsible for conceptualization, methodology, investigation, formal analysis, writing – original draft, visualization, and revising. B.A. contributed toward methodology, validation, and review. E.V. contributed to methodology, validation, and review. D.A.G. contributed toward conceptualization, methodology, validation acquisition and analysis of the AFM data and writing and review. M.R. contributed toward methodology and validation. C.S.T. contributed toward methodology and supervision. S.L. provided facility for investigation and validation. S.D. provided validation, supervision, writing review, and editing. I.R. was responsible for conceptualization, validation, supervision, editing of final document, and funding acquisition.

## Data Availability Statement

The data that support the findings of this study are available from the corresponding author upon reasonable request.

## Keywords

bacterial cellulose (BC), nanofibers, polyhydroxyalkanoates, tissue engineering

Received: February 15, 2025
Revised: April 11, 2025
Published online:

[1] B. Lukasiewicz, P. Basnett, R. Nigmatullin, R. Matharu, J. C. Knowles, I. Roy, *Acta Biomater.* **2018**, *71*, 225.
[2] E. Asare, D. Gregory, A. T. R. Fricker, E. Marcello, A. Paxinou, C. S. Taylor, J. Haycock, I. Roy, *Their Processing and Biomedical Applications* **2020**, *28*, 331.
[3] M. P. Raut, E. Asare, S. Mohamed, E. N. Amadi, I. Roy, *Int. J. Mol. Sci.* **2023**, *24*, 986.
[4] O. I. Kalaoglu-Altan, H. Baskan, T. Meireman, P. Basnett, B. Azimi, A. Fusco, N. Funel, G. Donnarumma, A. Lazzeri, I. Roy, S. Danti, K. De Clerck, *Materials* **2021**, *14*, 4907.
[5] J. Xie, X. Li, Y. Xia, *Macromol. Rapid Commun.* **2008**, *29*, 1775.
[6] L. R. Lizarraga-Valderrama, C. S. Taylor, F. C. Claeyssens, J. W. Haycock, J. C. Knowles, I. Roy, *J. Tissue Eng. Regener. Med.* **2019**, *13*, 1581.
[7] N. Bhardwaj, S. C. Kundu, *Biotechnol. Adv.* **2010**, *28*, 325.
[8] A. Greiner, J. H. Wendorff, *Angew. Chem. Int. Ed.* **2007**, *46*, 5670.
[9] P. Basnett, R. K. Matharu, C. S. Taylor, U. Illangakoon, J. I. Dawson, J. M. Kanczler, M. Behbehani, E. Humphrey, Q. Majid, B. Lukasiewicz, R. Nigmatullin, P. Heseltine, R. O. C. Oreffo, J. W. Haycock, C. Terracciano, S. E. Harding, M. Edirisinghe, I. Roy, *ACS Appl. Mater. Interfaces* **2021**, *13*, 32624.
[10] J. G. De la Ossa, S. Danti, J. Esposito Salsano, B. Azimi, V. Tempesti, N. Barbani, M. Digiacomo, M. Macchia, M. J. Uddin, C. Cristallini, R. Di Stefano, *Molecules* **2022**, *21*, 6208.
[11] J. G. De la Ossa, A. Fusco, B. Azimi, J. Esposito Salsano, M. Digiacomo, M. B. Coltelli, K. De Clerck, I. Roy, M. Macchia, A. Lazzeri, G. Donnarumma, *Appl. Sci.* **2021**, *28*, 4006.
[12] Z. Zhang, J. Hu, P. X. Ma, *Adv. Drug Delivery Rev.* **2012**, *64*, 1129.
[13] T. G. Kim, T. G. Park, *Biotechnol. Prog.* **2006**, *22*, 1108.
[14] F. Asghari, M. Samiei, K. Adibkia, A. Akbarzadeh, S. Davaran, *Artif. Cells, Nanomed., Biotechnol.* **2017**, *45*, 185.
[15] P. Basnett, K. Y. Ching, M. Stolz, J. C. Knowles, A. R. Boccaccini, C. Smith, I. C. Locke, T. Keshavarz, I. Roy, *React. Funct. Polym.* **2013**, *73*, 1340.
[16] D. A. Gregory, C. S. Taylor, A. T. R. Fricker, E. Asare, S. S. V. Tetali, J. W. Haycock, I. Roy, *Trends Mol. Med.* **2022**, *8*, 03331.
[17] P. Basnett, B. Lukasiewicz, E. Marcello, H. K. Gura, J. C. Knowles, I. Roy, *Microb. Biotechnol.* **2017**, *10*, 1384.
[18] S.-T. Yang, *Bioprocessing for value-added products from renewable resources: new technologies and applications*, Elsevier, Amsterdam **2011**.
[19] I. Noda, P. R. Green, M. M. Satkowski, L. A. Schechtman, *Biomacromolecules* **2005**, *6*, 580.
[20] H. J. Tang, S. Z. Neoh, K. Sudesh, *Front. Bioeng. Biotechnol.* **2022**, *10*, 1057067.
[21] Y.-F. Lee, N. Sridewi, S. Ramanathan, K. Sudesh, *Int. J. Biotechnol. Wellness Ind.* **2015**, *4*, 103.
[22] C. J. Brigham, A. J. Sinskey, *Int. J. Biotechnol. Wellness Ind.* **2012**, *1*, 52.
[23] L. R. Lizarraga-Valderrama, R. Nigmatullin, C. Taylor, J. W. Haycock, F. Claeyssens, J. C. Knowles, I. Roy, *Eng. Life Sci.* **2015**, *15*, 612.
[24] R. Nigmatullin, C. S. Taylor, P. Basnett, B. Lukasiewicz, A. Paxinou, L. R. Lizarraga-Valderrama, J. W. Haycock, I. Roy, *Regenerative Biomaterials* **2023**, *10*, 10.
[25] S. V. P. Bhavana V. Mohite, in *New and Future Developments in Microbial Biotechnology and Bioengineering*, (Ed: V. K. Gupta), Elsevier, Amsterdam **2016**, pp. 31–40.
[26] V. Raghavendran, E. Asare, I. Roy, *Bacterial cellulose: Biosynthesis, production, and applications* **2020**, *77*, 89.
[27] D. Gregory, L. Tripathi, A. T. R. Fricker, E. Asare, I. Orlando, V. Raghavendran, I. Roy, *Mater. Sci. Eng.: R: Rep.* **2021**, *145*, 100623.
[28] C. S. Taylor, M. Behbehani, A. Glen, P. Basnett, D. A. Gregory, B. B. Lukasiewicz, R. Nigmatullin, F. Claeyssens, I. Roy, J. W. Haycock, *ACS Biomater. Sci. Eng.* **2023**, *9*, 1472.
[29] F. Acevedo, P. Villegas, V. Urtuvia, J. Hermosilla, R. Navia, M. Seeger, *Int. J. Biol. Macromol.* **2018**, *106*, 692.
[30] F. Cerrone, T. Pozner, A. Siddiqui, P. Ceppi, B. Winner, M. Rajendiran, R. Babu, H. S. Ibrahim, B. J. Rodriguez, J. Winkler, K. J. Murphy, K. E. O'Connor, *Materials Science and Engineering C-Materials for Biological Applications* **2020**, *111*, 111.
[31] J. Li, J. N. Chen, Z. X. Peng, N. B. Chen, C. B. Liu, P. Zhang, X. Zhang, G. Q. Chen, *ACS Appl. Mater. Interfaces* **2023**, *15*, 364.
[32] W. Li, N. Cicek, D. B. Levin, S. Liu, *Int. J. Polym. Mater. Polym. Biomater.* **2019**, *68*, 499.
[33] X. H. Zhao, Y. N. Niu, C. H. Mi, H. L. Gong, X. Y. Yang, J. S. Y. Cheng, Z. Q. Zhou, J. X. Liu, X. L. Peng, D. X. Wei, *J. Polym. Sci.* **2021**, *59*, 1994.
[34] Y. Zhuikova, V. Zhuikov, V. Varlamov, *Polymers* **2022**, *14*, 5549.
[35] A. Cherpinski, S. Torres-Giner, J. Vartiainen, M. S. Peresin, P. Lahtinen, J. M. Lagaron, *Cellulose* **2018**, *25*, 1291.
[36] K. Peranidze, T. V. Safronova, N. R. Kildeeva, *Polymers* **2023**, *15*, 1174.
[37] M. A. Naeem, Q. Siddiqui, A. Leroy, M. R. Khan, Q. F. Wei, *J. Ind. Text.* **2021**, *51*, 380.
[38] I. Chiulan, D. M. Panaitescu, A. N. Frone, M. Teodorescu, C. A. Nicolae, A. Casarica, V. Tofan, A. Salageanu, *J. Biomed. Mater. Res., Part A.* **2016**, *104*, 2576.
[39] S. Rahmani, Z. Khoubi-Arani, S. Mohammadzadeh-Komuleh, M. Maroufkhani, in *Handbook of Nanocelluloses: Classification, Properties, Fabrication, and Emerging Applications*, (Ed: A. Barhoum), Springer International Publishing, Cham **2020**, pp. 1–34.
[40] G. Agoda-Tandjawa, S. Durand, S. Berot, C. Blassel, C. Gaillard, C. Garnier, J.-L. Doublier, *Carbohydr. Polym.* **2010**, *80*, 677.
[41] N. Olaru, N. Anghel, P. Pascariu, G. Ailiesei, *J. Appl. Polym. Sci.* **2019**, *136*, 47772.
[42] K. Liu, Z. Huang, J. Dai, Y. Jiang, G. Yang, Y. Liu, C. Lin, Y. Lv, M. Liu, *Chem. Eng. J.* **2020**, *382*, 122775.
[43] W. Chen, H. Ma, B. Xing, *Int. J. Biol. Macromol.* **2020**, *158*, 1342.
[44] P. Silva, C. Prieto, J. Lagarón, L. Pastrana, M. Coimbra, A. Vicente, M. Cerqueira, *Food Hydrocolloids* **2021**, *118*, 106761.
[45] Z. Ali Raza, S. Abid, I M. Banat, *Int. Biodeterior. Biodegrad.* **2018**, *126*, 45.
[46] N. Jacquel, N. Jacquel, C.-W. Lo, H.-S. Wu, Y.-H. Wei, S. S. Wang, *Solubility of Polyhydroxyalkanoates by Experiment and Thermodynamic Correlations*, AIChE Journal, Wiley-Blackwell **2007**, pp. 2704–2714.
[47] C. Stefanescu, W. H. Daly, I. I. Negulescu, *Carbohydr. Polym.* **2012**, *87*, 435.
[48] K S. Lefroy, B S. Murray, E. Michael, *J. Phys. Chem. B* **2021**, *125*, 8205.
[49] S. Xu, J. Zhang, A. He, J. Li, H. Zhang, C. C. Han, *Polymer* **2008**, *49*, 2911.
[50] Z. M. Huang, M. Kotaki, S. Ramakrishna, S. Kumar, *J. Appl. Polym. Sci.* **2003**, *89*, 1450.

 

[51] ELECTROSPINNING, https://www.nanoscience.com/techniques/electrospinning/ (accessed: April 2025).
[52] J. Xue, T. Wu, Y. Xia, *APL Mater.* **2018**, *6*, 120902.
[53] L. Chen, C. Yan, Z. Zheng, *Mater. Today* **2018**, *21*, 38.
[54] A. Zareidoost, M. Yousefpour, B. Ghaseme, A. Amanzadeh, *J. Mater. Sci.: Mater. Med.* **2012**, *23*, 1479.
[55] M. L. D. Lorenzo, M. Gazzano, M. C. Righetti, *Macromolecules* **2012**, *45*, 5684.
[56] J. A. P. Aguilar, J. M. Franco, I. D. Otero, R. B. Benítez, *Waste Biomass Valorization* **2024**, *15*, 4221.
[57] M. Poletto, H. Ornaghi, A. Zattera, *Thermal Decomposition of Natural Fibers: Kinetics and Degradation Mechanisms* **2015**, https://doi.org/10.1002/9781119117711.ch21.
[58] J. George, K. V. Ramana, S. N. Sabapathy, J. H. Jagannath, A. S. Bawa, *Int. J. Biol. Macromol.* **2005**, *37*, 189.
[59] B. Surma-Slusarska, S. Presler, D. Danielewicz, *Fibres Text. East. Eur.* **2008**, *16*, 108.
[60] V. V. Hlady, J. Buijs, *Curr. Opin. Biotechnol.* **1996**, *7*, 72.
[61] Y. Sun, Z. Xing, Y. Xue, K. Mustafa, A. Finne-Wistrand, A. C. Albertsson, *Biomacromolecules* **2014**, *15*, 1259.
[62] S. Hestrin, M. Schramm, *Biochem. J.* **1954**, *58*, 345.
[63] R. Nigmatullin, C. S. Taylor, P. Basnett, B. Lukasiewicz, A. Paxinou, L. Lizarraga Valderrama, J. Haycock, I. Roy, *Regener. Biomater.* **2023**, *10*, rbad063.
[64] S. P. Alappil, D. Peiris, G. J. Langley, J. M. Herniman, *J. Biotechnol.* **2007**, *127*, 475.
[65] B. Azimi, H. Maleki, V. Gigante, R. Bagherzadeh, A. Mezzetta, M. Milazzo, L. Guazzelli, P. Cinelli, A. Lazzeri, S. Danti, *Cellulose* **2022**, *29*, 3079.
[66] B. Azimi, M. Milazzo, S. Danti, *Frontiers in Bioengineering and Biotechnology* **2021**, *9*, 9.
[67] B. Azimi, A. Rasti, A. Fusco, T. Macchi, C. Ricci, M A. Hosseinifard, L. Guazzelli, G. Donnarumma, R. Bagherzadeh, M. Latifi, I. Roy, *Tissue Eng., Part A* **2024**, *30*, 25.
[68] M. Behbehani, A. Glen, C. S. Taylor, A. Schuhmacher, F. Claeyssens, J. W. Haycock, *International Journal of Bioprinting.* **2018**, *4*, 4.
[69] M. F. Daud, K. C. Pawar, F. Claeyssens, A. J. Ryan, J. W. Haycock, *Biomaterials* **2012**, *33*, 5901.
[70] C. S. Taylor, *Materials Science and Engineering*, University of Sheffield, UK **2018**.
[71] E. Altun, M. O. Aydogdu, S. O. Togay, A. Z. Sengil, N. Ekren, M. E. Haskoylu, E. T. Oner, N. A. Altuncu, G. Ozturk, M. Crabbe-Mann, J. Ahmed, O. Gunduz, M. Edirisinghe, *Eur. Polym. J.* **2019**, *114*, 98.
[72] R. Protz, A. Lehmann, J. Ganster, H.-P. Fink, *Carbohydr. Polym.* **2021**, *251*, 117027.
[73] X. Chen, X. Chen, X.-M. Cai, S. Huang, F. Wang, *ACS Sustainable Chem. Eng.* **2018**, *6*, 2898.
[74] J. Garemark, X. Yang, X. Sheng, O. Cheung, L. Sun, L. A. Berglund, Y. Li, *ACS Nano* **2020**, *14*, 7111.
[75] J. Cai, L. Zhang, *Macromol. Biosci.* **2005**, *5*, 539.
[76] A. Xu, J. Wang, H. Wang, *Green Chem.* **2010**, *12*, 268.

 